群馬県立自然史博物館研究報告 (28)：1－14，2024
Bull.Gunma Mus.Natu.Hist. (28)：1－14，2024

Original Article

A new species of Late Miocene balaenopterid, *Incakujira fordycei,* from Sacaco, Peru

Kimura Toshiyuki[1] and Hasegawa Yoshikazu[1,2]
[1]*Gunma Museum of Natural History, 1674-1 Kamikuroiwa, Tomioka, Gunma 370-2345, Japan*
(*kimura@gmnh.pref.gunma.jp*)
[2]*Iida City Museum, 2-655-7 Otemachi, Iida, Nagano 395-0034, Japan*

Abstract: We describe a new specimen of the Balaenopteridae from the upper Miocene, Pisco Formation, Peru. The holotype specimen is nearly a complete skeleton and most of the bones are preserved in articulated. Moreover, the holotype skull retains a rack of baleen in near-life position. Here we refer this specimen as a new species of the genus *Incakujira, I. fordycei* sp. nov. This new specimen will expand our knowledge of the paleobiodiversity and disparity of the balaenopterids. The vertebral and baleen plate morphology imply that *I. fordycei* was an agile swimmer with feeding on variety of diets (evasive and also non-evasive prey items).

Key words: Cetacea, Balaenopteridae, *Incakujira fordycei*, Miocene, Mysticeti, Peru, Pisco Formation

INTRODUCTION

Baleen whales (Cetacea: Mysticeti), which are the largest living carnivores, are represented by four families that contain 15 living species (Committee on Taxonomy, 2023). Balaenopteridae is the most speciose and widely distributed living family, containing eight living species of rorquals, *Balaenoptera*, and a single living humpback whale, *Megaptera novaeangliae*. The traditional separation of rorquals and humpback at the subfamily level reflects the phenetic disparity between the two genera and indeed living *Balaenoptera* seems to be a structurally conservative genus (Fordyce and Barnes, 1994; Fordyce and Muizon, 2001). Modern species of the Balaenopteridae are generally cosmopolitan and inhabit all major oceans, from the tropics to polar zones in both hemispheres (Jefferson et al., 2015). They are sympatrically distributed with several species of balaenopterids, and they occupy important ecological niches in each area of the oceans (e.g., García-Vernet et al., 2021). This might also be the case for fossil relatives.

In the recent decades, many studies have described a new member of the Balaenopteridae and shed light on their diversity and disparity in the past oceans (e.g., Bisconti, 2007, 2010; Bosselaers and Post, 2010; Bisconti and Bosselaers, 2016, 2020; Marx and Kohno, 2016; Bisconti et al., 2019, 2020a, b, 2022; Leslie et al., 2019; Tanaka and Watanabe, 2019). Demere et al. (2005) reviewed the taxonomy of the extant and fossil balaenopterids. However, the relationships among balaenopterids remain unclear, and their evolutionary history has not been fully documented.

The Pisco Formation of Peru is renowned as "fossil-Lagerstätten" in yielding an outstanding fossil collection of marine vertebrates. With regard to cetaceans, previous literature indicates the abundance of fossil cetaceans from Peru (Muizon 1984, 1988, 1993; Pilleri 1989, 1990; Muizon et al., 1999; Bianucci et al., 2015; Esperante et al., 2015; Bosio et al., 2021; Collareta et al., 2021; Ochoa et al., 2021; Bianucci and Collareta, 2022). This is also the case for fossil balaenopterids of the Pisco Formation, but only a few specimens of balaenopterids have been formally described in previous studies (Pilleri, 1989; Marx and Kohno, 2016; Bisconti et al., 2022). The aim of this article is to identify and describe a new fossil species in the family Balaenopteridae from the Pisco Formation, Peru. The species is represented by a remarkably complete skeleton and will expand our knowledge of the paleobiodiversity and disparity of balaenopterids. The LSID for this publication is: urn:lsid:zoobank.org:pub:892A697D-CC27-4296-AD27-3251BB1E3262

MATERIAL AND METHODS

The specimen comprises an almost-complete skeleton (GMNH-PV-159) displayed at the Gunma Museum of Natural History, Tomioka, Gunma, Japan (Figure 1). Dorsal and lateral surfaces are accessible, but the ventral details of the skull and skeleton are covered by matrix (cemented quartzose fine sandstone) or mounting material. Descriptions below consider the right or left element, whichever is more-informative. The surface mesh of the cranium was created by capturing surface details using the Artec Spider/ Eva handheld 3D scanners (Artec Group, Luxembourg). The captured data were processed with standard workflow using Artec Studio 13.

Institutional Abbreviations.—GMNH, Gunma Museum of Natural History, Tomioka, Gunma, Japan; GNHM, Gamagori Natural History Museum, Gamagori, Aichi, Japan.

SYSTEMATICS

Suborder Mysticeti Flower, 1864
Family Balaenopteridae Gray, 1864
Genus *Incakujira* Marx and Kohno, 2016

Type species. *Incakujira anillodefuego* Marx and Kohno, 2016
Other species included. *Incakujira fordycei* sp. nov.
Remarks. *Incakujira* is placed in Balaenopteridae because: the frontals and plate-like anterior extensions of the parietals form a steep walled intertemporal region which passes laterally to extensive subhorizontal supraorbital processes of the frontals; each maxilla expands abruptly at the posterior of the rostrum, forming a robust posterolaterally directed process that is closely sutured to the frontal, and which has an excavated and posteriorly-concave profile. Incakujira is excluded from modern genera of the Balaenopteridae (*Balaenoptera* and *Megaptera*) because it lacks: expanded flat posterior apices of the maxillae; it has long rather than short nasals; and it has a longer, narrower intertemporal region on which parietals (or interparietal) are clearly exposed dorsally.

Incakujira fordycei sp. nov.

(Figures 1-9, Tables 1-3)

LSID. urn:lsid:zoobank.org:act:1E056092-7F09-46F6-BD92-52B8B4778890
Holotype. GMNH-PV-159, a nearly complete skeleton (Figure 1). With permissions of the Peruvian authorities, this specimen was excavated by Black Hills Institute of Geological Research, Inc. in 1987 and was subsequently exported to Japan, Gunma

Submitted : October 12, 2023; Accepted : December 6, 2023

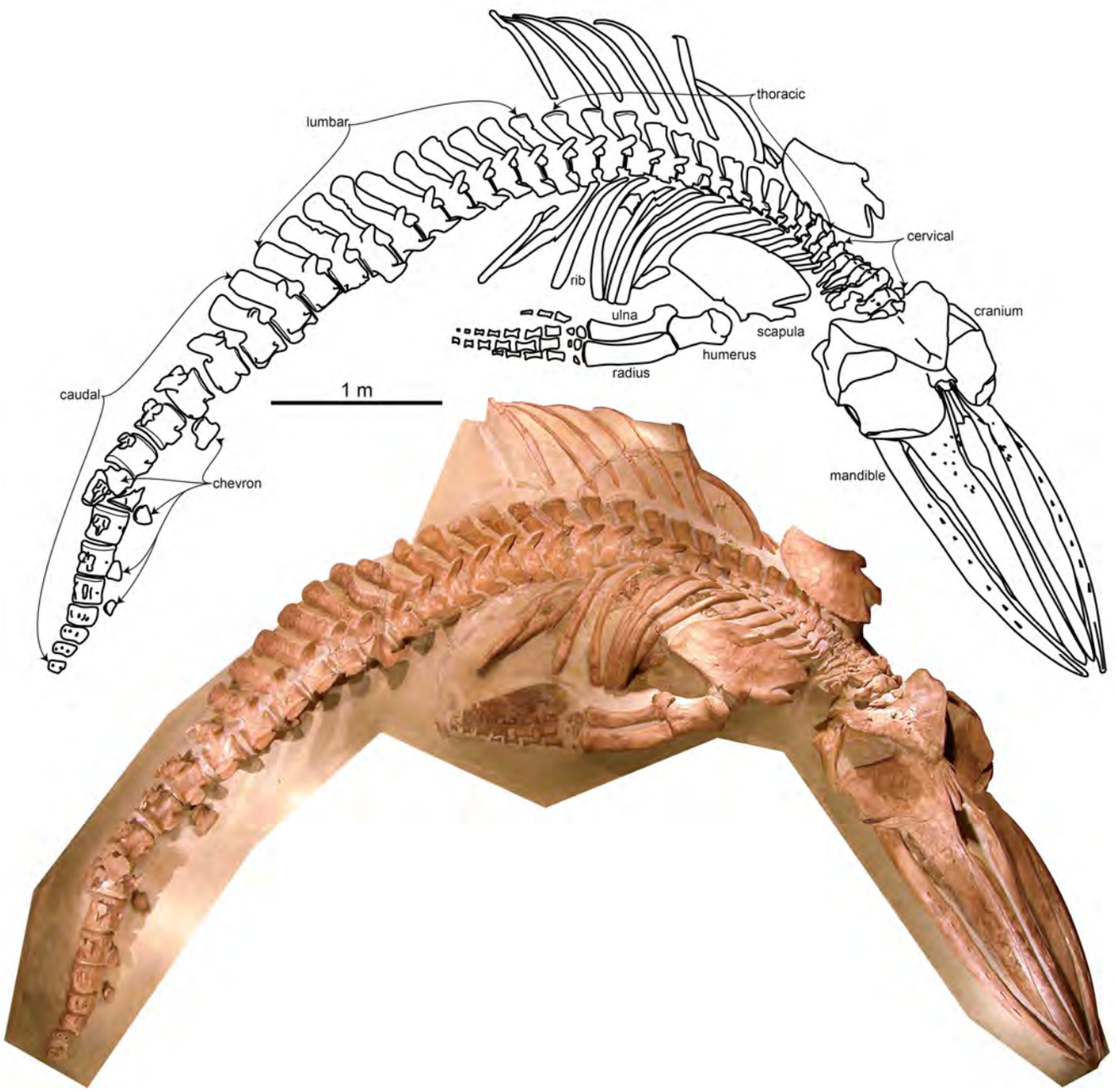

Figure 1. *Incakujira fordycei* sp. nov., GMNH-PV-159, holotype. Photograph and illustration of the skeleton as currently on display at Gunma Museum of Natural History, Tomioka, Gunma, Japan.

Prefectural Museum of History. In 1996, the specimen was transferred to Gunma Museum of Natural History with its inauguration.

Locality and Horizon. The holotype was found from Aguada de Lomas, Sacaco, Arequipa Department, Republic of Peru in 1987. It was recovered from the Aguada de Lomas (AGL) locality of Muizon and DeVries (1985). Three radiometric K-Ar ages from two tuff layers (samples 44 and 45 of Muizon and Bellon, 1986) are indicated an age between 8.85 and 7.93 Ma (Muizon and Bellon, 1986), and this provides an approximate age for the lowermost sedimentary successions of the AGL vertebrate-level of Muizon and DeVries (1985) (Ochoa et al., 2022). The age for the uppermost level of the sedimentary successions at Aguada de Lomas is estimated as 6.2-5.6 Ma by diatom biostratigraphy (Ochoa et al., 2022). Muizon (1988:19) estimated the age of AGL vertebrate-level of Muizon and DeVries (1985) as ca. 7.5-7.0 Ma. Ehret et al. (2012) suggested the possible range of 7.5-7.3 Ma for AGL vertebrate-level based on strontium dating. Lambert and Muizon (2013) suggested that the AGL vertebrate-level corresponds to the bed LM9 to LM11 of Brand et al. (2011) and estimated the age as ca. 8-7 Ma. Thus, as a conservatively, we consider the age of the holotype as ca. 8-7 Ma here.

Etymology. Honors Prof. R. Ewan Fordyce, in recognition of his enduring and influential contributions to the study of cetacean paleobiology. The epithet also honors his great contributions to the early phase of our project. GMNH officially invited Prof. Fordyce in 2004, and the authors discussed with him the morphology and phylogeny of the holotype, GMNH-PV-159. This discussion has yielded a pivotal insight into our understanding of the specimen.

Diagnosis. Differs from I. *anillodefuego* in: less telescoped cranium with anterior end of nasal locating anterior to level of antorbital notch and posterior end of nasal locating at anterior 1/4 of orbit; transversally narrower ascending process

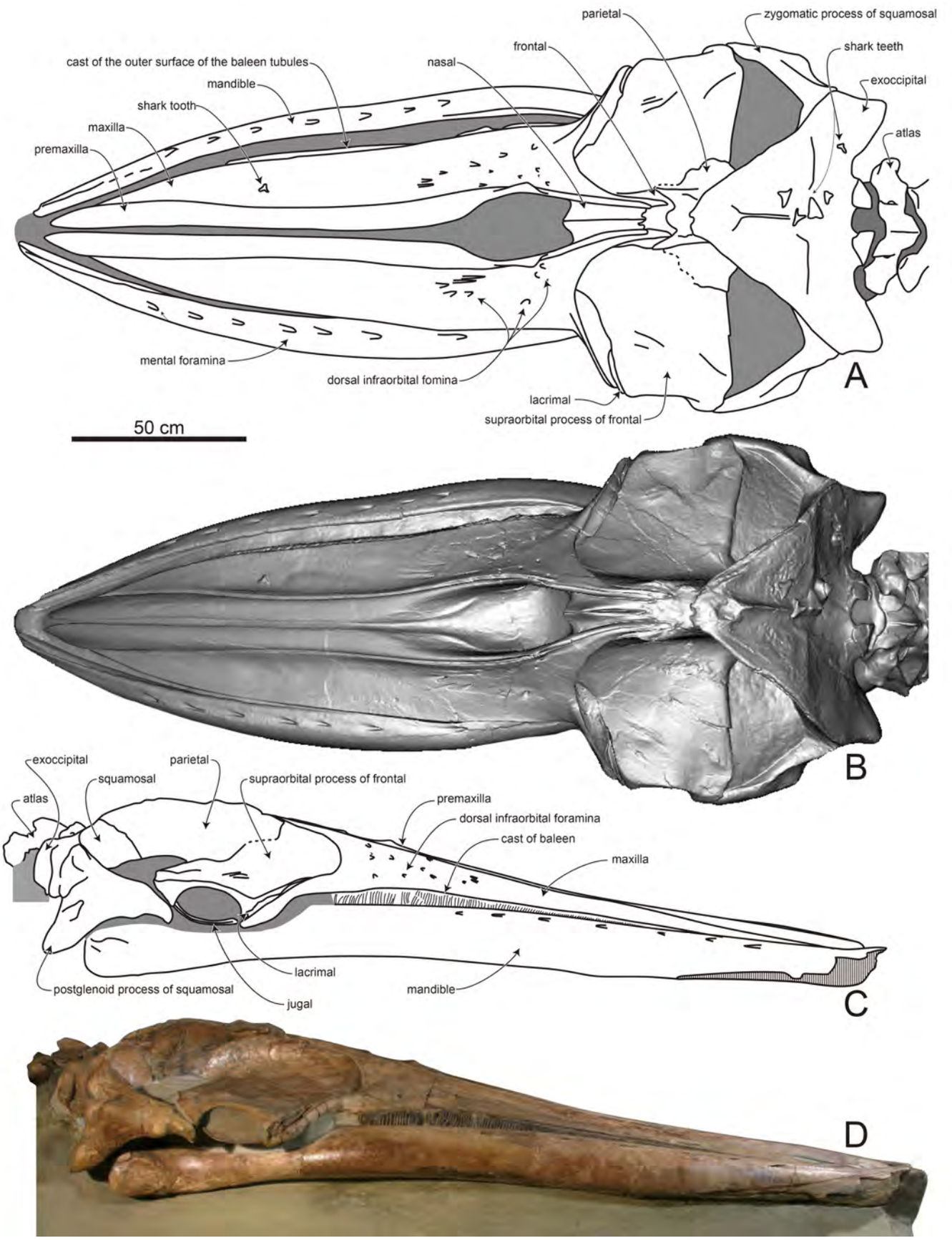

Figure 2. *Incakujira fordycei* sp. nov., GMNH-PV-159, holotype. Photograph, 3D model and illustrations of the skull in **A**, **B**, dorsal and **C**, **D**, lateral views. Grey represents areas covered by matrix.

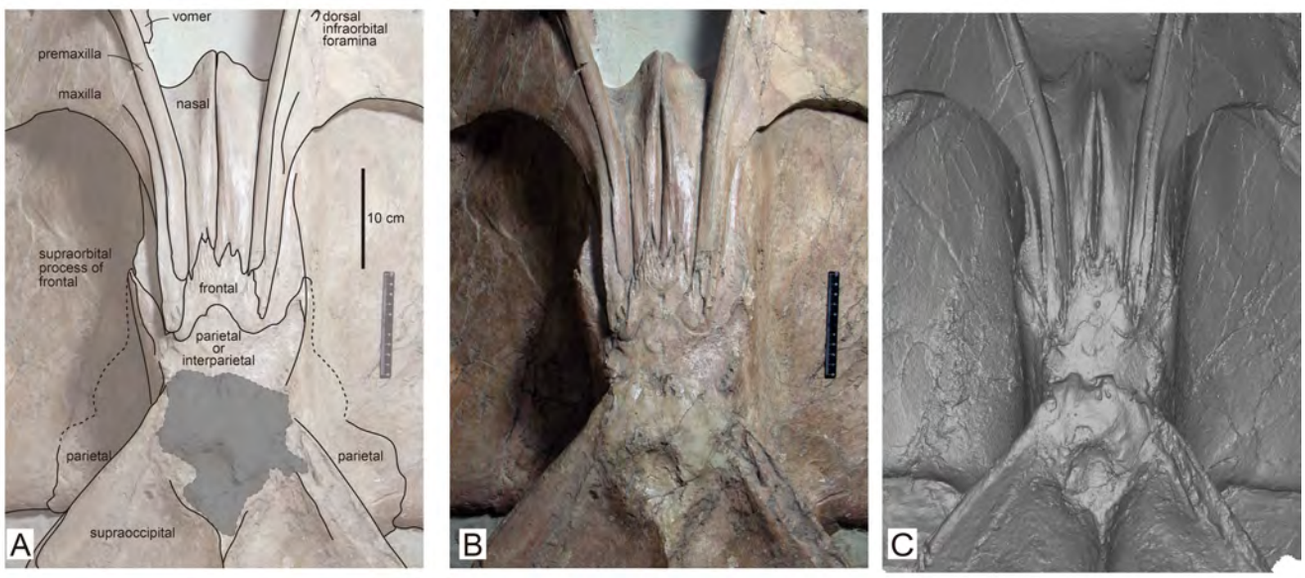

Figure 3. *Incakujira fordycei* sp. nov., GMNH-PV-159, holotype. Interpretative illustration (**A**), photograph (**B**) and 3D model (**C**) of the vertex in dorsal view. Grey represents areas reconstructed at around the apex of the supraoccipital.

of premaxilla; ascending processes of maxilla and premaxilla extending further posteriorly to posterior end of nasals; more slender and elongate nasal bones; large exposure of parietal and/or interparietal on flat-topped intertemporal region; parietal broadly covers posteromedial part of supraorbital process of frontal; thickened knob-like anterodorsal part of parietal.

Remarks. *I. fordycei* is placed in the genus *Incakujira* because of the following combination of characters: twisted postglenoid process; narrow, attenuated ascending process of the maxilla; well-defined external occipital crest; triangular protuberance on the supraoccipital; and lacking a squamosal crease (Marx and Kohno, 2016).

DESCRIPTION

Skeleton. The skeleton is 9.22 m long along the curve of the spine as preserved, with the skull (cbl = 2377 mm) forming 25.8 % of body length, although several distal-most caudal vertebrae are apparently missing (Figure 1). This skull-body length ratio is slightly higher than that of modern rorquals based on the measurements in True (1904). For example, in *Balaenoptera acutorostrata*, the proportion ranges from 20.6 % to 23.1 %, except for the extraordinary smallest juvenile individual (body length = 302.3 cm), which represents the ratio of 26.9 %. As discussed later, the holotype specimen was considered as a juvenile or young subadult, which may explain their relatively higher skull-body length ratio. The total body length is also estimated to be 10.47 m by using the formula of Pyenson and Sponberg (2011) for stem Balaenopteroidea. In this case, the skull corresponds to 22.7 % of the body length. Sixteen shark teeth of *Cosmopolitodus hastalis* are also preserved with the holotype specimen (Takakuwa, 2014).

Skull. Visible parts of the skull are essentially complete (Figures 2); the skull retains lacrimals, jugals and much of the right rack of baleen in near-life position, but it is slightly distorted so that the dorsal part is a little displaced to the left. The right mandible is in life position, articulated with the postglenoid process and closely approximating the right rack of baleen and rostrum in the manner seen in fresh stranded minke whale carcasses, but the left mandible is displaced slightly toward midline. Bone surfaces in places show minor fractures. There is some reconstruction at the apex of the supraoccipital (grayed area in Figure 3A). The left tympanic bulla is partly visible (Figure 4) and suggests the periotic and tympanic bulla are preserved in situ. But, those are hidden by matrix and not able to observe.

The rostrum is long, more or less parallel-sided rather than subtriangular, and forms ca. 33 % of skull length; it is conspicuously narrower than the orbital breadth of the cranium. The bony nares open forward of the cranium. The cranium is wider than long, and is dominated by extensive ventrally-depressed supraorbital processes and a forward-thrust triangular supraoccipital. The flat-topped intertemporal region is longer than wide, with parietals (and/or interparietal) exposed dorsally, and rostral bones do not closely approach the supraoccipital. This is clearly contrast to that of *I. anillodefuego*, which has the rostral bones closely approached to the supraoccipital. The temporal fossae are wide and anteroposteriorly narrow, albeit with ventral profiles hidden by matrix. Minor left-right differences in bones in the intertemporal region probably reflect fluctuating asymmetry compounded by minor compression; there is no evidence of true directional asymmetry. Measurements of the cranium is shown in Table 1.

Premaxilla. Both premaxillae are almost complete; they closely approximate each other but do not fully roof the mesorostral groove. On the rostrum, each premaxilla is more or less parallel-sided, with a flat dorsal surface which is the widest about 1/4 length from the acutely-pointed apex. The premaxilla is slightly elevated above the adjacent maxilla for all of its length. Toward the posterior of the rostrum, the outer border of the premaxilla rises to form a narrow crest bounding the nares, while the broad more-medial part slopes posteriorly into the nares. Slightly behind the middle of the nares, each premaxilla has a small prominent narrow dorsal crest (= triangular eminence of Marx and Kohno, 2016; narial crest of the premaxilla of Tanaka et al., 2019) that is triangular and hooked backwards in lateral view, and is bent outward to overhang the premaxillary-maxillary suture. Similar structure is also found in *I. anillodefuego* (triangular eminence of Marx and Kohno, 2016). Perhaps the rather open suture here carried a blood vessel. Further posteriorly, the narrow ascending process of the premaxilla extends back beyond the level of the nares (Figure 3), partly overlying the adjacent maxilla, but it does not reach the posterior limit of the maxilla. Both premaxillae have lost bone, at least a few mm to possibly 10+ mm, from their apices.

Maxilla. The smooth dorsal surface of the maxilla is almost flat anteriorly, but posteriorly on the rostrum it slopes down and outwards. Slight postmortem distortion is apparent in anterior and dorsal views (Figures 2 and 5). In the middle part of the

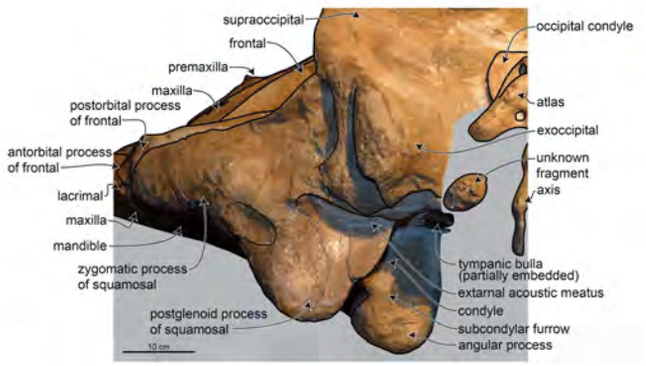

Figure 4. *Incakujira fordycei* sp. nov., GMNH-PV-159, holotype. Photograph with interpretative line drawing of the skull in posterolateral view. Grey represents areas covered by matrix.

maxilla (dorsal view), the lateral and medial edges are subparallel, while the anterior quarter is attenuated. The maxilla slightly widens at the level of the nares, and, just behind the level of the nares, it widens rapidly to bound the laterally-extended supraorbital process. An indistinct horizontal groove (presumably for the facial nerve) is present at the abrupt curve between the rostral and preorbital parts of the maxilla. The dorsal outer preorbital half of the maxilla has a robust, prominent laterally-directed posterior maxillary crest, behind which the maxilla is more or less continuous with the dorsal surface of the supraorbital process of the frontal. Here, the region of the frontomaxillary suture is not fissured. Posterolaterally, the maxilla has a robust thickened border that underlies both the lacrimal and the anterior process of the frontal (Figures 2 and 6). Ventrally, the thick edge of the maxilla passes medially into what appears to be a thinner infraorbital plate; details are hidden by matrix. On the dorsal surface, the posterior maxillary crest rises and curves dorsomedially and posteriorly, to roof a matrix-filled cavity into which the frontal extends, then passing back to form the ascending process. In dorsal view, the ascending process is clearly narrow rather than flattened and broad, and it folds over ridges of frontal in a serrate suture (Figure 3). The left process reaches the level of the frontal-parietal suture, but the right process does not, so that a small strip of frontal is exposed (Figure 3). A prominent crest that separates the dorsal and lateral surfaces of the ascending process is more obvious on the left than the right, perhaps because of compression. The dorsal infraorbital foramina open on the dorsal surface level with the middle to anterior of the nares, with 11 (possibly 12) on the right and 8 (possibly 9) on the left. Most of the foramina face anteriorly, but each maxilla has a larger posteriorly-directed foramen opening near the crest on the premaxilla (possibly primary dorsal infraorbital foramen of Marx et al., 2016). The right maxilla carries a rack of baleen (detailed below).

Nasals and nares. The nasals are robust, prominent and long, wide and medially elevated anteriorly, and flatter and more-parallel-sided posteriorly. There is a marked internasal suture. Anteriorly, each nasal is depressed laterally, and it has a concave anterior profile. Posteriorly, the dorsal surface has a distinct elongate groove. The nasofrontal suture is asymmetrical, but this is interpreted as fluctuating asymmetry without particular significance. Anteriorly, the nasal lies forward of the antorbital notch, while posteriorly it reaches the level of the anterior of the orbit, with the premaxilla and maxilla extending further posteriorly. This is in contrast to that of *I. anillodefuego*. In *I. anillodefuego*, the nasal is further posteriorly located, and the anterior and posterior extremities are at the level of the antorbital notch and the level of the mid-orbit, respectively. Laterally, the nasal is bounded wholly by premaxilla, but within the nares, the anterolateral corner of the nasal contacts another element - presumably maxilla (Figure 3). A larger bilateral element present further anteroventrally in the nares may be vomer. The nares face anteriorly and slightly dorsally.

Lacrimal. Both lacrimals are preserved in situ and wedged between the supraorbital process of the frontal and the lateral process of the maxilla. Left lacrimal is completely preserved (Figure 6), and the right one is slightly damaged at its lateral tip. The lacrimal is medially thin and thickened laterally. A sharp transverse crest is observed on its dorsal surface.

Jugal. Both jugals are well-preserved almost in situ, but slightly displaced medially. In ventral view, the jugal is relatively broad transversally, and it widens anteriorly (Figure 6). In lateral view, it is shallowly arched and contributes a ventral border of the orbit.

Frontal. The orbit is shallow and elongate, with robust anterior and posterior processes; the latter is closely approached by an opposing surface on the zygomatic process of the squamosal. Each flat-topped supraorbital process is broadly exposed, and

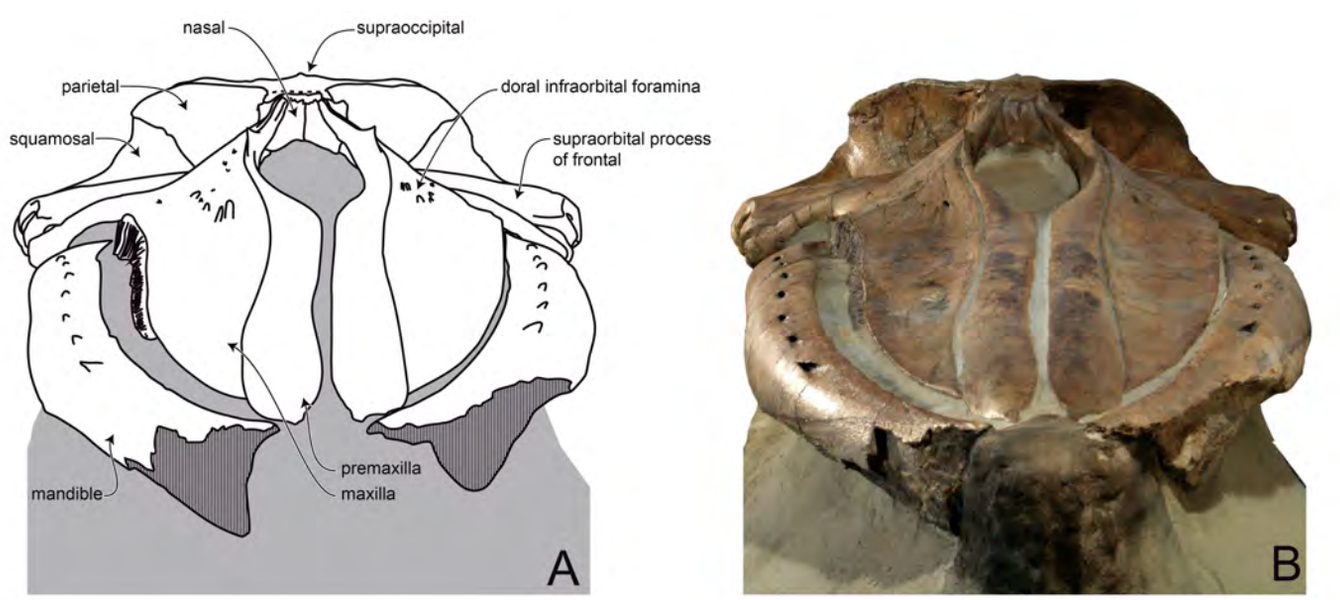

Figure 5. *Incakujira fordycei* sp. nov., GMNH-PV-159, holotype. Illustration (**A**) and photograph (**B**) of the skull in anterior view.

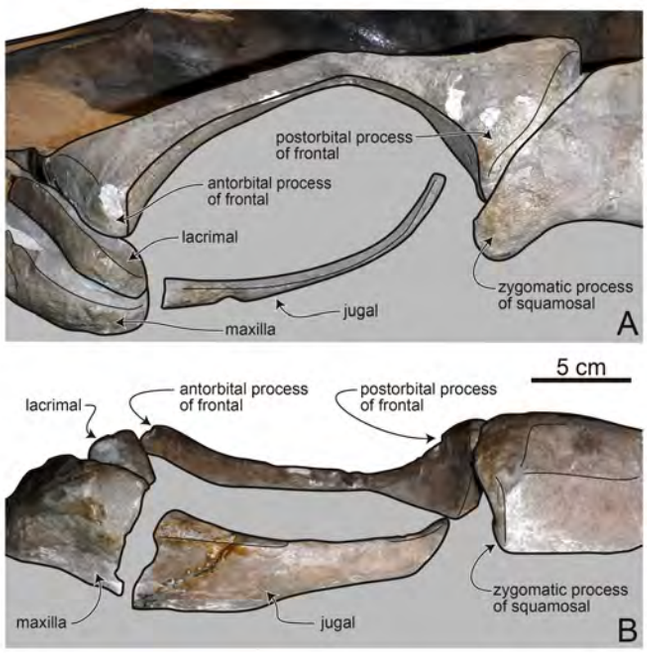

Figure 6. *Incakujira fordycei* sp. nov., GMNH-PV-159, holotype. Photograph with interpretative line drawing of the left orbit in lateral (**A**) and ventral (**B**) views. Grey represents area covered by matrix.

gently tilted laterally; anteromedially, the process rises abruptly towards the flat-topped intertemporal region, but the element is not exposed posteromedially where the parietal, which overlaps the frontal, forms the wall of the intertemporal region. The anteromedial part of the frontal extends forward into the matrix-filled cavity under the posterior maxillary crest, nearly level with the anterior of the nasals. Here, the frontal has a faint but distinct posterolaterally directed ridge, oriented towards another oblique ridge in the middle part of the supraorbital process (Figures 2 and 7). Yet another oblique ridge arises a little further posteriorly, trending towards a prominent bend on the outer part of the posterior edge of the process. The ridges appear to be symmetrical on left and right; they probably reflect different origins for parts of the temporalis muscles. A similar pattern of the ridges is also found in *Archaeobalaenoptera eusebioi* (Bisconti et al., 2022). Laterally, a prominent ridge near the orbital border probably marks the outer limit of temporalis origins. In dorsal view, the inner three-quarters of the posterior border of the supraorbital process is robust and rounded vertically as well as concave posteriorly. The posteromedial part of the supraorbital process is broadly covered by the parietal (Figures 2 and 3). More-ventral details are hidden by matrix. In the intertemporal region, a narrow subhorizontal shelf is present on both frontals, between the ascending process of the maxilla and the projecting apex of the parietal (Figure 3). On the better-preserved right side, the shelf is grooved, suggesting vessels and/or muscle origins, and slightly concave. There is no obvious interfrontal suture posterior to the nasals, although there is an anteriorly-concave suture-like structure associated with some more-posteriorly placed medially-aligned foramina and fissures. The frontoparietal suture is distinct and simple but obscured in the midline.

Parietal. The parietals (or possibly interparietal) form the posterior of the flat-topped intertemporal region between the reconstructed apex of the supraoccipital and the posterior rostral elements, frontals, and nasals (Figure 3). Laterally, a plate-like part of each parietal project forwards from under the supraoccipital, forming part of the wall of the intertemporal region. Each plate-like part of the parietal attains roughly the level of the posterior of the nasals, and it is thickened dorsally to form a conspicuous crest. On both sides, the frontoparietal suture can be traced down onto the lateral wall of the intertemporal and can also be traced forwards from the posteromedial part of the supraorbital region, but the path is obscured across the mid-length of the supraorbital process. The parietal clearly forms the posteromedial part of the supraorbital region, including some of the rounded temporal crest. The parietal broadly covers the posteromedial part of the supraorbital process of the frontal; thus, this part of the parietal is visible in dorsal view (Figures 2 and 3). Unsurprisingly, the parietal forms the vertical to overhanging wall of the braincase above the temporal fossa and forms the outer part of the nuchal crest where it meets the supraoccipital at a prominent suture. The parieto-squamosal suture within the temporal fossa is subvertical.

Supraoccipital and exoccipital. The supraoccipital shield is roughly triangular in its anterior two-thirds. Although a few centimeters at the apex is damaged, it is clear that the bone lacks the blunt wide form as observed in recent rorquals. The apex extends well forward relative to the level of the orbit, beyond the apex of the zygomatic process of the squamosal. The nuchal crest, which carries the parietal/supraoccipital suture, is prominent. In roughly its posterior third, above the region of the postglenoid process and meatus and delimited by bilateral low oblique ridges, the supraoccipital becomes more parallel-sided as its margins descend towards the exoccipitals. The dorsal surface is concave in transverse profile and gently convex in anterior-posterior profile. A prominent anterior sagittal crest becomes indistinct posteriorly. On either side of the crest, the bone surface has semi-regular stippled shallow depressions up to 10 mm across; whether these are original or postmortem is

Figure 7. *Incakujira fordycei* sp. nov., GMNH-PV-159, holotype. Photograph of the right supraorbital process of frontal in dorsal view. Arrows indicate the ridges on the supraorbital process of the frontal.

Table 1. Measurements of the cranium of the holotype, GMNH-PV-159 (in mm). Abbreviations: L, left; R, right; +, less than true value.

Bizygomatic width	1048	
Condylobasal length	2377	
Maximum width of temporal fossa	381 (R)	380 (L)
Bicondylar width	233	
Anteroposterior diameter of orbit	180 (R)	167 (L)
Maximum width of anterior portion of premaxilla	81 (R)	81 (L)
Width of premaxill at level of posterior end of nasal		15 (L)
Width of premaxilla at mid-lenght of nasal	14 (R)	17 (L)
Width of ascending process of maxilla at tip	14+ (R)	16 (L)
Maximum length of nasal	241	
Combined width of nasals at anterior border	126	
Combined width of nasals at posterior tip	47	
Width of nasal at anteiror tip	63 (R)	65 (L)
Width of nasal at tip of narial process of frontal	30 (R)	22 (L)
Maximum width of narial fossa	180	
Rostrum width at base	593	
Rostrum length	1615	
Transverse width at mid-orbit	964	
Transverse width between exoccipitals	674	

uncertain. Unlike *I. anillodefuego*, the triangular protuberance, which is located lateral to the sagittal crest, is not so obvious in *I. fordycei.*

The foramen magnum is broadly exposed to dorsal view, and the condyles are prominent, with sharp edges. Ventral details are obscured by matrix and the articulated atlas. The dorsal apex of the condyles is developed far forward so that the condyle is well exposed to dorsal view. Laterally, the supraoccipital passes imperceptibly into the robust paroccipital process of the exoccipital, which is most obvious in lateral view (Figure 4). Each exoccipital is thick anteroposteriorly, with a rounded and rugose lateral end. The exoccipital is not particularly extended ventrally or laterally. The suture between the exoccipital and squamosal is prominent and deep. The external end of the exoccipital projects backward slightly beyond the level of the occipital condyle. This is clearly contrast to *I. anillodefuego*, the external end of the exoccipital of the latter remains to the level of the posterior surface of the occipital condyle

Squamosal. Each robust and massive zygomatic process of the squamosal is directed anterolaterally at ca. 30 degrees to the skull axis. Presumably, it was contacted by the jugal (both jugals are slightly separated from the squamosals). As seen in lateral view, the ventral surface of the zygomatic process is more or less flat anteriorly, slopes gently posteriorly, and passes into the postglenoid process. Anteriorly, the ventral surface has a small notch in its profile near the apex. The apex is deflected anteroventrally. In lateral view, there are two large depressions on the lateral surface (Figures 2 and 4): one on the base of the postglenoid process slightly below the level of the external acoustic meatus, and the other high on the squamosal between the temporal and nuchal crests. Forwards, a large, smooth indistinct projection is developed on the base of the zygomatic process. The postglenoid process is robust and rotated anterolaterally. The twisting is less marked than that of *I. anillodefuego*. From the ventral apex of the postglenoid process, a sharp crest develops as the process rises medially and dorsally towards the auditory canal. Ventrally, the left side shows the external acoustic meatus (Figure 4). Dorsally, the posterior half of the squamosal carries a prominent narrow supramastoid crest that extends posteromedially to meet the nuchal crest. That part of the squamosal near the exoccipital is prominently rugose, presumably forming an origin for part of the neck muscles. Details within the fossa are obscured by matrix; the exposed posterior border of the squamosal shows no evidence of a squamosal cleft which, in crown-*Balaenoptera*, would normally be visible above the level of the matrix. There is no exposure of the alisphenoid in the visible parts of the wall of the temporal fossa.

Mandible. Both mandibles are almost complete except for its proximal part which are broken off on its ventral and anterior sides (Figure 2). As stated above, both mandibles are preserved nearly in life position and are closely approximated to the corresponding part of the rostrum. The mandible is bowed laterally with reflection at the region of the coronoid process, although the coronoid process is covered by the matrix. In lateral view, the ventral profile of the mandible is shallowly arched dorsally. A remnant of the gingival groove is preserved on the dorsal margin of the proximal part of the mandible. Seven mental foramina are preserved along the dorsolateral surface of the left and right mandibles. All foramina open into an anteriorly directed sulci. The lateral surface of the mandible convex dorsoventrally, and the point of the greatest convexity is below the midline at the middle part of the mandible. At the middle part of the mandible, the medial and lateral surfaces of the mandible meet ventrally and form a well-defined angular edge. The condyle is oriented posteriorly. The lateral border of the condyle projects well beyond the lateral surface of the adjacent portion of the ramus. A shallow subcondylar furrow is developed on the posterior surface of the mandible between the condyle and angular process (Figure 4). It is also visible in lateral view. The angular process is small and only slightly extended posteriorly beyond the level of the posterior surface of the condyle.

Baleen. As stated above, the right rack of baleen is preserved in near-life position (Figure 8). The right rack of baleen comprises more than 120 plates along the rostrum. This plate structure is interpreted as a cast of the outer surface of the baleen tubules; thus, the thickness of the sediment indicates the gaps between the adjacent baleen plates (Gioncada et al., 2016). Each plate, which is considered as the gap between each baleen plate, is 2.9-7.1 mm thick. The thickness of each plate roughly increases posteriorly. The average thickness of the individual plate of the 20 plates at the anterior-most and posterior-most portions of the rack is 3.7 and 5.4 mm, respectively. Considering a baleen plate thickness of 1.0-1.5 mm (Marx and Kohno, 2016), the plate density can be estimated as 1.5-2.1 plates/cm. This value is roughly in the range of the plate density of *B. edeni* and *B. acutorostrata* (Young, 2012).

Vertebrae. Forty-four vertebrae were associated with the skeleton and identified as seven cervical, 13 thoracic, 10 lumbar, and 14 caudal vertebrae (Figure 1). Apparently, there were

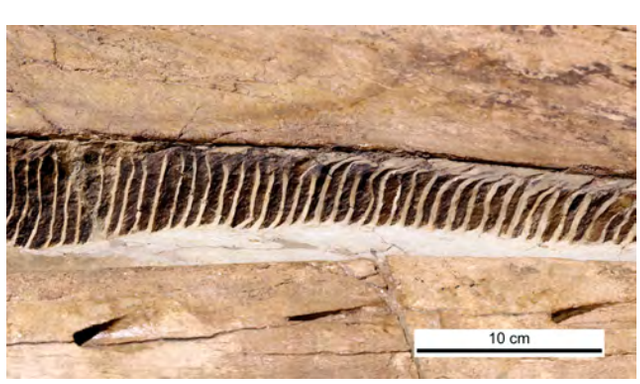

Figure 8. *Incakujira fordycei* sp. nov., GMNH-PV-159, holotype. Photograph of the cast of baleen plate.

Table 2. Measurements of the vertebrae of the holotype, GMNH-PV-159 (in mm). Abbreviations: Ca, caudal vertebra; CH, centrum, height; CL, centrum length; CW, centrum width; e, estimated; L, lumbar vertebra; T, thoracic vertebra; *, doubling half-width.

	CL	CH	CW
T10	151		
T11	170		
T12	162		
T13	165		
L1	163		
L2	158		
L3	169		
L4	173		
L5	178		
L6	186		
L7	189		
L8	165		
L9	173		
L10	198		

	CL	CH	CW
Ca1	210		
Ca2	211		
Ca3	207	198	
Ca4	207	200	
Ca5	204		
Ca6	205	191	206
Ca7	198	166	240*
Ca8	186	218	184
Ca9	170	180e	182
Ca10	148	178e	167
Ca11	111	139	152
Ca12	82		131
Ca13	71		
Ca14	64		

several additional terminal caudal vertebrae that were lost. The composition of the vertebra is similar to that of *I. anillodefuego* (C7, T12-13, L9, Ca18+) (Marx and Kohno, 2016). Almost all the preserved vertebrae are in a life-position and articulated one another. The neural spine increases its height posteriorly, reaching the highest at the posterior lumbar vertebrae, and then decreases the height posteriorly. The anteroposterior diameter of the neural spine also increases posteriorly. The posterior lumbar and anterior caudal vertebrae represent a widest transverse diameter, and then it decreases posteriorly. Five chevron bones are preserved with the skeleton. Measurements of the vertebrae are shown in Table 2.

Rib. Thirteen right and nine left ribs were associated with the holotype skeleton. Most of which, particularly the right ribs, are preserved nearly in a life-position. They are roughly associated with the transverse costal facet of the corresponding thoracic vertebrae. The ribs are generally robust, and the transverse diameter is wide. The transverse diameter of the distal part of the seventh right rib is 79 mm. In lateral view, the outline of the central ribs is sigmoidal.

Forelimb bones. The right forelimb bones are almost completely preserved nearly in a life-position, whereas only a scapula is preserved in the left (Figure 1). The scapula is elongated anteroposteriorly. *I. fordycei* has an apparently longer profile of the scapula in comparison with *I. anillodefuego*; the ratio of the maximum length/maximum height is 1.77-2.03 for *I. fordycei* and 1.63-1.69 for *I. anillodefuego* (Marx and Kohno, 2016). The posterior border is directed almost posteriorly, which meets the dorsal border through a nearly right angle. On the contrary, the anterior border is directed anterodorsally. The dorsal margin of the scapula represents a markedly uneven surface, indicating a former presence of a cartilaginous element. As typical in the Balaenopteridae, the supraspinous fossa is narrow. The acromion is large and directs anterodorsally. Although the distal part is broken, the remaining part suggests that the acromion was distally expanded. The glenoid fossa is shallowly concave. The coracoid process projects from the anterior border of the glenoid fossa. Although the distal part of the coracoid process is broken off in both scapulae, the remaining base of the coracoid process indicates that it directs anteromedially and slightly ventrally.

The right humerus, ulna, and radius are almost completely preserved (Figure 9). The humerus is much shorter than the ulna and radius as typical in balaenopterids.

It retains epiphyses with visible sutures. The head is markedly convex and directed posterodorsally. Anteromedial to the head is a greater tubercle that projects anteromedially. A shallow fossa

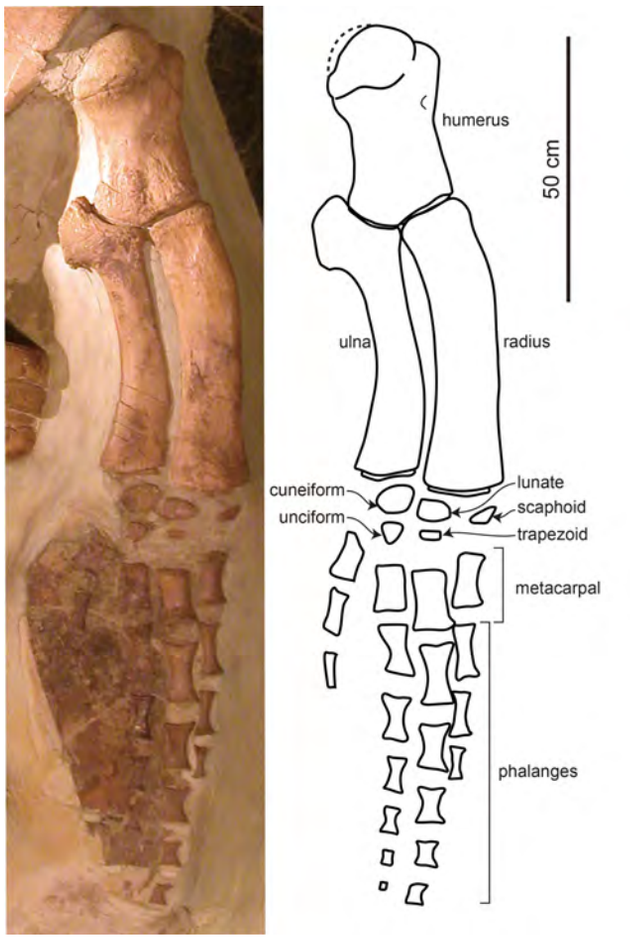

Figure 9. *Incakujira fordycei* sp. nov., GMNH-PV-159, holotype. Photograph and illustration of the right forelimb bones.

is observed on the lateral surface of the shaft and interpreted as an infraspinous fossa. The radius and ulna retain proximal and distal epiphyses with visible sutures. A margin of the olecranon process of the radius represents an uneven surface, indicating the former presence of a cartilaginous element. Measurements are shown in Table 3.

The patterns of the carpal elements of the holotype are similar to those in living balaenopterids (Cooper et al., 2007). Five carpal elements are preserved and identified as scaphoid, lunate, cuneiform for the proximal row and trapezoid and unciform for the distal row (Figure 9). The holotype has four digital rays as typical in balaenopterids. Each digital ray preserves three, five, six, and two phalanges craniocaudally, and one or more distal elements may be lost. Therefore, the holotype clearly exhibits hyperphalangy, and the holotype of *I. fordycei*, together with other balaenopterid fossils from Peru (e.g., Pilleri, 1989, 1990), is one of the oldest direct evidence of the hyperphalangy in cetaceans (Cooper et al., 2007). Each phalangeal bone has an hourglass outline, and it is remarkably constricted at the middle in lateral view. The matrix around the digital rays is smooth and dark brown/black colored in a shape of a flipper-like outline. This might perhaps be interpreted as a cast of the outer surface of the soft tissue flipper.

PHYLOGENETIC ANALYSIS

To investigate the phylogenetic position of *I. fordycei*, we performed a phylogenetic analysis by using the matrix of Tanaka et al. (2020), which was derived from the matrix of

Table 3. Measurements of the forelimb bones of the holotype, GMNH-PV-159 (in mm).

Right scapula, maximum length	847
Right scapula, maximum height	417
Left scapula, maximum length	793
Left scapula, maximum height	448
Humerus, maximum proximodistal length including epiphyses	377
Humerus, minimum diameter of shaft in lateral view	164
Humerus, greatest anteroposterior diameter of proximal end	219
Humerus, greatest anteroposterior diameter of distal end	197
Radius, maximum proximodistal length	528
Radius, maximum anteroposteior diameter of proximal end	125
Radius, maximum anteroposteior diameter of distal end	149
Ulna, maximum proximodistal length excluding olecranon	476
Ulna, maximum anteroposterior diameter of the proximal end excluding olecranon	94
Ulna, maximum anteroposterior diameter of the dsital end	119

Marx and Kohno (2016), Marx et al. (2017), and Tanaka and Watanabe (2019). With the addition of *I. fordycei*, the matrix consists of 100 taxa and 273 morphological characters (online supplementary file). We have performed a phylogenetic analysis with TNT version 1.5 (Goloboff and Catalano, 2016) using the New Technology Search with recover minimum length tree = 1000 times. All the characters were treated as unordered and unweighted.

Our analysis resulted in 4298 shortest trees, each with a length of 1307 steps, a consistency index of 0.277 and a retention index of 0.737. Figure 10 shows the strict consensus tree of the resulting trees. The tree topology is virtually identical to that of Marx and Kohno (2016) and Tanaka et al. (2020) in recovering the monophyly of Eomysticetidae, Balaenidae, Cetotheriidae, and Balaenopteridae+Eschrichtiidae. *I. fordycei* is clustered with *I. anillodefuego*, with sharing the following characters: posteriorly convergent lateral margins of the nasal (Chr. 74); concaved anterior half of the dorsal surface of the supraoccipital (Chr. 115); twisted postglenoid process in ventral view (Chr. 121); and sigmoidal outline of central ribs in lateral view (Chr. 252). *I. fordycei*, together with *I. anillodefuego*, is placed within the crown group of the Balaenopteridae. The clade is supported by the following characters: presence of the separation of the posterior portion of the nasals along the sagittal plane by the narial process of the frontal (Chr. 77); external occipital crest present and running all the way along the supraoccipital shield (Chr. 116); presence of attachment of the anterior process of the periotic to pars cochlearis (Chr. 145); absence of distinct ridge delimiting insertion surface of the tensor tympani on the medial side of the anterior process of the periotic (Chr. 160); absence of median promontorial groove on the medial side of the pars cochlearis (Chr. 163); caudal tympanic process of the periotic which is narrowly separated or contacted to the crista parotica in posteromedial view (Chr. 164).

DISCUSSION

Ontogeny

The ontogenetic fusion of the vertebral epiphyses in cetaceans is initiated in the anterior cervical and posterior caudal vertebrae and is completed in middle/posterior thoracic vertebrae (Kato, 1988; Moran et al., 2015). In the holotype of *I. fordycei* (GMNH-PV-159), the both anterior and posterior epiphyses of the preserved posterior-most four caudal vertebrae (Ca11-14) and posterior epiphysis of the tenth caudal vertebra are firmly fused to the respective centrum, whereas all other vertebral epiphyses of the caudal, lumbar, and posterior thoracic vertebrae are distinctly visible (the centrum of all cervical and anterior thoracic vertebrae are covered by sediment). This clearly suggest GMNH-PV-159 was immature individual. This is also supported by the unfused epiphyses of the humerus, radius, and ulna in GMNH-PV-159. The closed occipital joints suggest that GMNH-PV-159 is not classified as a young calf individual (Walsh and Berta, 2011). These features suggest that GMNH-PV-159 could be interpreted as an old calf to a young subadult.

Marx and Kohno (2016) concluded that the holotype of *I. anillodefuego* (GNHM-Fs-098-12) was a subadult because the proximal epiphyses of the humeri are firmly ankylosed to the shafts and the vertebral epiphyses are firmly fused with the centrum in most of the vertebrae, except for the posterior thoracic and anterior lumbar vertebrae. Based on the pattern of the fusion of epiphyses in the vertebrae and forelimb bones, it is suggested that the holotype of *I. fordycei* was ontogenetically younger than that of *I. anillodefuego*. However, the size of the cranium is slightly larger in the holotype of *I. fordycei* (2377 mm for *I. fordycei* versus 2260 mm for *I. anillodefuego* in condylobasal length). This might perhaps reflect the average body size difference between the two species in the genus *Incakujira*.

Swimming style and feeding strategy of *I. fordycei*

During the process of their secondary adaptation to the life in water, cetaceans have acquired extensive structural and functional modifications in their locomotion style (e.g., Fish, 2001, 2016; Gingerich et al., 2019; Boessenecker et al., 2020). In the Neoceti, most of the thrust power for the swimming is generated by the oscillation of the fluke, which is induced by the motion of the axial skeleton (Buchholtz, 1998, 2001). This suggests that the pattern of the vertebral morphology could be a proxy for predicting their swimming performance. To investigate the evolution of the hydrodynamic performance in cetaceans, Buchholtz (2001) discussed the swimming style of the modern and fossil cetaceans based on the morphology of the vertebral centrum. The holotype of *I. fordycei* includes a virtually complete vertebral column, making it possible to discuss their hydrodynamic performance based on the vertebrate morphology.

Following Buchholtz (2001) and Kimura and Hasegawa (2008), we have examined the relative centrum length (centrum length divided by the average of centrum width and centrum height) of each vertebra for *I. fordycei* with six species of modern balaenopterids and one balaenid for comparison (Figure 11, Table 4). Considering that many of the vertebrae of the holotype of *I. fordycei* are still partially embedded in the matrix, only the centrum length, height, and width of the six caudal vertebrae could be measured (Table 2). Even though, we can precisely identify the exact position of each vertebra, which allows us to compare the relative centrum length of the holotype of *I. fordycei* with that of modern balaenopterids.

As discussed by Kimura and Hasegawa (2008), the relative centrum length in balaenopterids has two patterns, and the distinction of the relative centrum length among those patterns is the most apparent in the posterior thoracic to central caudal vertebrae (torso) (Figure 11). The first pattern is characterized by having a relatively short and nearly uniform relative centrum length in the torso (Kimura and Hasegawa, 2008). The centrum

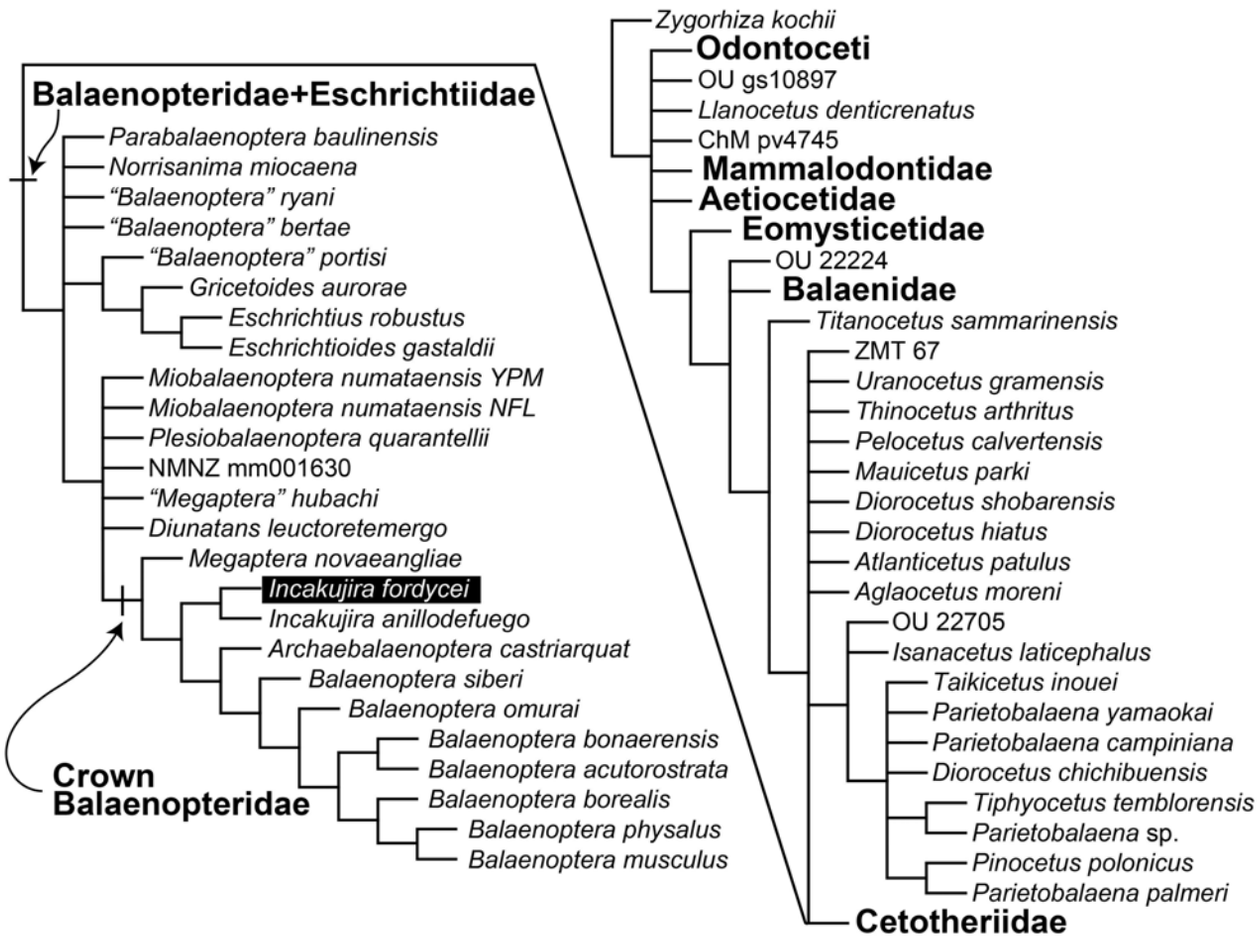

Figure 10. *Incakujira fordycei* sp. nov., GMNH-PV-159, holotype. Strict consensus tree. Clades in bold were collapsed.

is shorter than its height and width in all vertebrae (relative centrum length < 1.0). This type of vertebral column allows limited excursion of the flukes and represents a more reduced flexibility of the body (Buchholtz, 2001), which is a parameter associated with increased stability for swimming (Fish and Rohr, 1999). This pattern is found in *B. musculus*, *B. physalus*, and *Megaptera novaeangliae*. The second pattern is characterized by having a relatively long relative centrum length with an apparent peak in the torso (Kimura and Hasegawa, 2008). The centrum length exceeds its height and/or width in the torso (relative centrum length > 1.0). This type of vertebral column allows large dorsoventral movement of peduncle and flukes (Buchholtz, 2001). Longer relative centrum length also indicates the flexible movement of the body, which is a parameter associated with the maneuverability for swimming (Fish and Rohr, 1999). This pattern is developed in *B. acutorostrata*, *B. borealis*, and *B. edeni*. Kimura and Hasegawa (2008) referred the two abovementioned patterns as stability priority mode and maneuverability priority mode swimming, respectively. Furthermore, this trend in swimming performance in baleen whales is also suggested by the study using bio-logging and aerial photogrammetry (Segre et al., 2022).

To assess the effect of age/individual variations, the relative centrum length was also examined for the eight individuals of *B. acutorostrata* whose body length ranges from 4.8 to 9.8 m (Figure 12, Table 4). The relative centrum length represents a certain level of the age/individual variations. However, all of the individuals have a relatively long relative centrum length with an apparent peak in the torso and the centrum length exceeds its height and/or width in the torso (relative centrum length > 1.0). Therefore, all the examined individuals are classified as the same swimming style (maneuverability priority mode swimming).

Balaenopterids have utilized a variety of food resources in each species. Blue whale almost exclusively feed on krill (Sears and Perrin, 2018). Fin whale also almost exclusively feed on krill in the Southern Hemisphere, although they also feed on a variety of organisms in the Northern Hemisphere (Aguilar and García-Vernet, 2018). Interestingly, the right whales have similar pattern of a relative centrum length of stability priority mode balaenopterids (Figure 11), and they feed entirely on non-evasive prey (e.g., copepods). Their stability priority mode swimming might be related to their preference for a non-evasive prey. By contrast, minke whale feed on a variety of non-evasive and evasive prey items (Perrin et al., 2018). Bryde's whale feed primarily on pelagic schooling fish (Kato and Perrin, 2018). Sei whale has a fine structure of baleen, which allows them to skim feed on copepods, but they also feed on a wide range of prey, including shoals of fish (Kawamura, 1980; Horwood, 2018). In general, it seems that the balaenopterids of stability priority mode swimming prefer to feed on non-evasive prey, whereas those of maneuverability priority mode swimming feed a variety of diets (non-evasive and evasive prey items). Although this specialization includes exceptions: i.e., the humpback whale represents a relative centrum length of stability priority mode, but has a generalist diet by their unique feeding strategy (bubble net feeding by using a large forelimb for maneuver swimming) (Clapham, 2018), it might demonstrate a general tendency of balaenopterids.

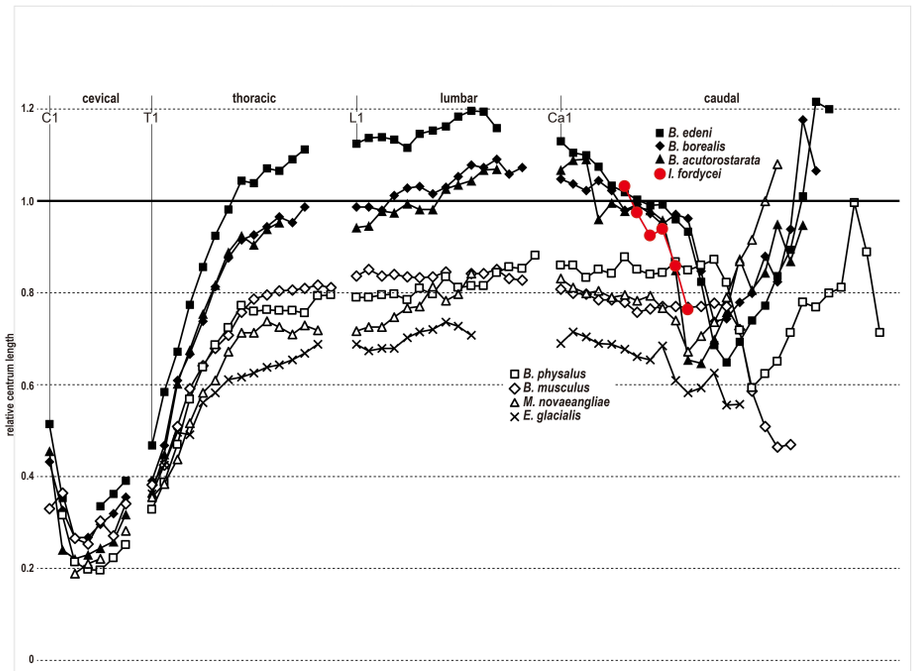

Figure 11. Centrum dimensions in relative centrum length of the holotype of *I. fordycei* sp. nov. with the balaenopterids and *Eubalaena glacialis*.

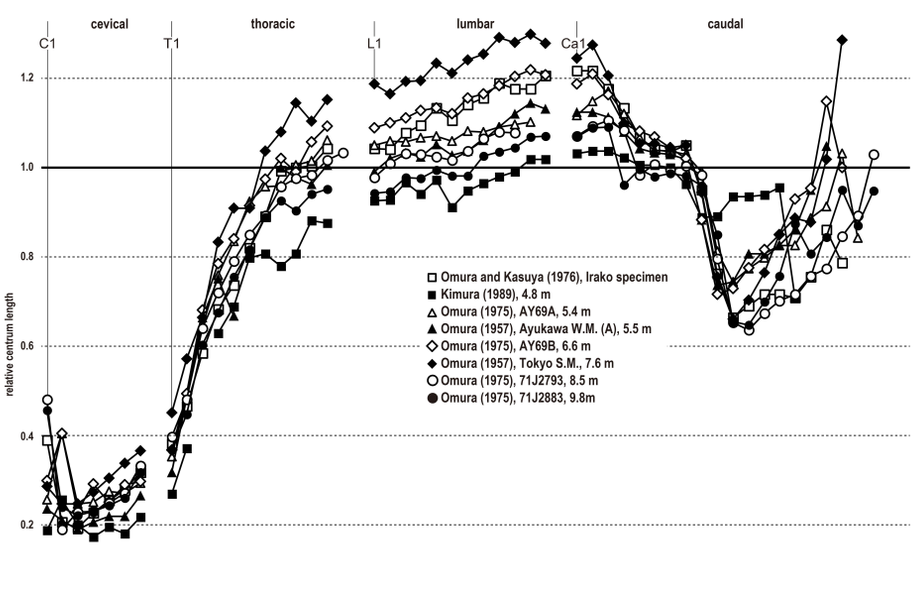

Figure 12. Centrum dimensions in relative centrum length of *Balaenoptera acutorostrata*.

The centrum length of the holotype of *I. fordycei* in the anterior caudal vertebrae is relatively long, and an apparent peak occurs in the torso vertebrae (Figure 11). This clearly suggests the vertebral pattern of *I. fordycei* is classified as maneuverability priority mode swimming. This may imply that *I. fordycei* feed not only on non-evasive but also on evasive prey items.The morphology of the baleen plate generally reflects their prey items (Pivorunas, 1976; Young, 2012). As mentioned above, the plate density of *I. fordycei* is in rage of that of *B. edeni* and *B. acutorostrata*, and the pattern of the relative centrum length of these species is similar to that of *I. fordycei* (maneuverability priority mode swimming). This collateral evidence suggests that *I. fordycei* was an agile swimmer that feed on variety of diets: i.e., evasive and non-evasive prey items.

ACKNOWLEDGEMENTS

We would like to express our sincere gratitude to R. Ewan Fordyce of Otago University for his great contribution to this project. Without his suggestions and the discussions with him, we would not have been able to complete this project. We would like to thanks to Y. Tanaka of Osaka Museum of Natural History for reviewing the manuscript and making suggestions leading to its improvement. We would also like to express our thanks to Y. Takakuwa of GMNH, C.-H. Tsai of National Taiwan University and Marilyn Fordyce for their help; M. Iijima of Asia Nature Vision for the photograph of the holotype skeleton; P. L. Larson and R. Farrar of Black Hills Institute for providing a detail information of the fossil locality. This study was partially supported by Prefectural Museum Research Fund by Gunma

Table 4. List of the specimens in Figures 11 and 12.

Figure 11	Specimen ID	Body length (m)	Sexual status	Sex	Reference
Balaenoptera acutorostrata	71J2883	9.8	Mature	Female	Omura (1975)
Balaenoptera borealis		15.3	Mature	Female	Nishiwaki and Kasuya (1971)
Balaenoptera edeni	77N62	14.7	Mature		Omura et al. (1981)
Balaenoptera musculus	66 P1	18.6	Mature	Male	Omura et al. (1970)
Balaenoptera physalus		14.6			Dwight (1872)
Megaptera novaeangliae		12.2	Mature		Struthers (1888)
Eubalaena glacialis	61A	17.0	Mature	Male	Omura et al. (1969)
Incakujira fordycei sp. nov.	GMNH-PV-159		Immature		present study

Figure 12	Specimen ID	Body length (m)	Sexual status	Sex	Reference
Balaenoptera acutorostrata	Irako specimen		Immature		Omura and Kasuya (1976)
Balaenoptera acutorostrata		4.8	Immature		Kimura (1989)
Balaenoptera acutorostrata	AY69A	5.4	Immature	Male	Omura (1975)
Balaenoptera acutorostrata	Ayukawa W.M. (A)	5.5	Immature	Male	Omura (1957)
Balaenoptera acutorostrata	AY69B	6.6	Immature	Male	Omura (1975)
Balaenoptera acutorostrata	Tokyo S.M.	7.6	Immature	Male	Omura (1957)
Balaenoptera acutorostrata	71J2793	8.5	Mature	Male	Omura (1975)
Balaenoptera acutorostrata	71J2883	9.8	Mature	Female	Omura (1975)

Prefectural Government during the fiscal year of 2003 and by JSPS KAKENHI Grant Numbers JP18K01110 to TK.

REFERENCES

Aguilar, A. and García-Vernet, R. (2018): Fin whale, *Balaenoptera physalus*. *In*, Würsig, B., Thewissen, J. G. M. and Kovacs, K. M. (eds.) Encyclopedia of Marine Mammals. Academic Press, London, p. 368-371.

Bianucci, G. and Collareta, A. (2022): An overview of the fossil record of cetaceans from the East Pisco Basin (Peru). *Bollettino della Società Paleontologica Italiana*, 61:19-60.

Bianucci, G., Di Celma, C., Landini, W., Post, K., Tinelli, C., Muizon, C. de, Gariboldi, K., Malinverno, E., Cantalamessa, G., Gioncada, A., Collareta, A., Gismondi, R.-S., Varas-Malca, R., Urbina, M. and Lambert, O. (2015): Distribution of fossil marine vertebrates in Cerro Colorado, the type locality of the giant raptorial sperm whale *Livyatan melvillei* (Miocene, Pisco Formation, Peru). *Journal of Maps*, 12:543-557.

Bisconti, M. (2007): A new basal balaenopterid whale from the Pliocene of Northern Italy. *Palaeontology*, 50:1103-1122.

Bisconti, M. (2010): A new balaenopterid whale from the Late Miocene of the Stirone River, Northern Italy (Mammalia, Cetacea, Mysticeti). *Journal of Vertebrate Paleontology*, 30:943-958.

Bisconti, M. and Bosselaers, M. (2016): *Fragilicetus velponi*: a new mysticete genus and species and its implications for the origin of Balaenopteridae (Mammalia, Cetacea, Mysticeti). *Zoological Journal of the Linnean Society*, 177:450-474.

Bisconti, M. and Bosselaers, M. (2020): A new balaenopterid species from the Southern North Sea Basin informs about phylogeny and taxonomy of *Burtinopsis* and *Protororqualus* (Cetacea, Mysticeti, Balaenopteridae). *PeerJ*, 8:e9570.

Bisconti, M., Damarco, P., Pavia, M., Sorce, B. and Carnevale, G. (2020b): *Marzanoptera tersillae*, a new balaenopterid genus and species from the Pliocene of Piedmont, north-west Italy. *Zoological Journal of the Linnean Society*, 192:1253-1292.

Bisconti, M., Munsterman, D. K. and Post, K. (2019): A new balaenopterid whale from the late Miocene of the Southern North Sea Basin and the evolution of balaenopterid diversity (Cetacea, Mysticeti). *PeerJ*, 7:e6915.

Bisconti, M., Munsterman, D. K., Fraaije, R. H. B., Bosselaers, M. E. J. and Post, K. (2020a): A new species of rorqual whale (Cetacea, Mysticeti, Balaenopteridae) from the Late Miocene of the Southern North Sea Basin and the role of the North Atlantic in the paleobiogeography of *Archaebalaenoptera*. *PeerJ*, 8:e8315.

Bisconti, M., Ochoa, D., Urbina, M. and Salas-Gismondi, R. (2022): *Archaebalaenoptera eusebioi*, a new rorqual from the late Miocene of Peru (Cetacea, Mysticeti, Balaenopteridae) and its impact in reconstructing body size evolution, ecomorphology and palaeobiogeography of Balaenopteridae. *Journal of Systematic Palaeontology*, 19:1129-1160.

Brand, L., Urbina, M., Chadwick, A., DeVries, T. J. and Esperante, R. (2011): A high resolution stratigraphic framework for the remarkable fossil cetacean assemblage of the Miocene/Pliocene Pisco Formation, Peru. *Journal of South American Earth Sciences*, 31:414-425.

Bosio, G., Collareta, A., Di Celma, C., Lambert, O., Marx, F. G., Muizon, C. de, Gioncada, A., Gariboldi, K., Malinverno, E., Malca, R. V., Urbina, M. and Bianucci, G. (2021): Taphonomy of marine vertebrates of the Pisco Formation (Miocene, Peru): Insights into the origin of an outstanding Fossil-Lagerstätte. *PLoS One*, 16:e0254395.

Bosselaers, M. and Post, K. (2010): A new fossil rorqual (Mammalia, Cetacea, Balaenopteridae) from the Early Pliocene of the North Sea, with a review of the rorqual species described by Owen and Van Beneden. *Geodiversitas*, 32:331-363.

Boessenecker, R. W., Churchill, M., Buchholtz, E. A., Beatty, B. L. and Geisler, J. H. (2020): Convergent evolution of swimming adaptations in modern whales revealed by a large macrophagous dolphin from the Oligocene of South Carolina. *Current Biology*, 30:3267-3273.E2

Buchholtz, E. A. (1998): Implications of vertebral morphology for locomotor evolution in early Cetacea. *In*, Thewissen, J. G. M. (ed.) Emergence of Whales. Plenum Press, New York, p. 325-351.

Buchholtz, E. A. (2001): Vertebral osteology and swimming style in living and fossil whales (Order: Cetacea). *Journal of Zoology*, 253:175-190.

Clapham, P. J. (2018): Humpback whale, *Megaptera novaeangliae*. *In*, Würsig, B., Thewissen, J. G. M. and Kovacs, K. M. (eds.) Encyclopedia of Marine Mammals. Academic Press, London, p. 489-492.

Collareta, A., Lambert, O., Marx, F. G., Muizon, C. de, Varas-Malca, R., Landini, W., Bosio, G., Malinverno, E., Gariboldi, K., Gioncada, A., Urbina, M. and Bianucci, G. (2021): Vertebrate Palaeoecology of the Pisco Formation (Miocene, Peru): Glimpses into the Ancient Humboldt Current Ecosystem. *Journal of Marine Science and Engineering*, 9:1188. https://doi.org/10.3390/jmse9111188

Committee on Taxonomy (2023): *List of marine mammal species and subspecies*. *Society for Marine Mammalogy* [online]. (Retrieved 2023-11-23) Available from https://marinemammalscience.org/science-and-publications/list-marine-mammal-species-subspecies/

Cooper, L. N., Berta, A., Dawson, S. D. and Reidenberg, J. S. (2007): Evolution of hyperphalangy and digit reduction in the cetacean manus. *The Anatomical Record*, 290:654-672.

Demere, T. A., Berta, A. and McGowen, M. R. (2005): The taxonomic and evolutionary history of modern balaenopteroid mysticetes. *Journal of Mammalian Evolution*, 12:99-143.

Dwight, T. (1872): Description of the whale (*Balaenoptera musculus* Acut.) in the possession of the society: with remarks on the classification of Fin whale. *Memoirs of the Boston Society of Natural History*, 2:203-230.

Ehret, D. J., Macfadden, B. J., Jones, D. S., DeVries, T. J., Foster, D. A. and Salas-Gismondi, R. (2012): Origin of the white shark *Carcharodon* (Lamniformes: Lamnidae) based on recalibration of the Upper Neogene Pisco Formation of Peru. *Palaeontology*, 55:1139-1153.

Esperante, R., Brand, L. R., Chadwick, A. V. and Poma, O. (2015): Taphonomy and paleoenvironmental conditions of deposition of fossil whales in the diatomaceous sediments of the Miocene/Pliocene Pisco Formation, southern Peru—A new fossil-lagerstätte. *Palaeogeography, Palaeoclimatology, Palaeoecology*, 417:337-370.

Fish, F. E. (2001): A mechanism for evolutionary transition in swimming mode by mammals. *In*, Mazin, J.-M. and Buffréil, V. de (eds.) Secondary Adaptation of Tetrapods to Life in Water. p. Verlag Dr. Friedrich Pfeil, München, p. 261-287.

Fish, F. E. (2016): Secondary Evolution of Aquatic Propulsion in Higher Vertebrates: Validation and Prospect. *Integrative and Comparative Biology*, 56:1285-1297.

Fish, F. E. and Rohr, J. J. (1999): Review of dolphin hydrodynamics and swimming performance. Technical Report 1801. SSC, San Diego, 136 pp.

Flower, W. H. (1864): Notes on the skeletons of whales in the principal museums of Holland and Belgium, with descriptions of two species apparently new to science. *Proceedings of The Zoological Society of London*, 1864:384-420.

Fordyce, R. E. and Barnes, L. G. (1994): The evolutionary history of whales and dolphins. *Annual Review of Earth and Planetary Sciences*, 22:419-455.

Fordyce, R. E. and Muizon, C. de (2001): Evolutionary history of cetaceans: a review. *In*, Mazin, J.-M. and Buffrénil, V. de (eds.) Secondary Adaptation of Tetrapods to Life in Water. Verlag Dr. Friedrich Pfeil, München, Germany, p. 169-233.

García-Vernet, R., Borrell, A., Víkingsson, G., Halldórsson, S. D. and Aguilar, A. (2021): *Ecological niche partitioning between baleen whales inhabiting Icelandic waters. Progress in Oceanography*, 199:102690.

Gingerich, P. D., Antar, M. S. M. and Zalmout, I. S. (2019): *Aegicetus gehennae*, a new late Eocene protocetid (Cetacea, Archaeoceti) from Wadi Al Hitan, Egypt, and the transition to tail-powered swimming in whales. *PLoS One*, 14:e0225391.

Gioncada, A., Collareta, A., Gariboldi, K., Lambert, O., Di Celma, C., Bonaccorsi, E., Urbina, M. and Bianucci, G. (2016): Inside baleen: Exceptional microstructure preservation in a late Miocene whale skeleton from Peru. *Geology*, 44:839-842.

Goloboff, P. A. and Catalano, S. A. (2016): TNT version 1.5, including a full implementation of phylogenetic morphometrics. *Cladistics*, 32:221-238.

Gray, J. E. (1864): Notes on the Whalebone-Whales; with a synopsis of the species. *The Annals and Magazine of Natural History*, 14:345-353.

Horwood, J. (2018): Sei whale, *Balaenoptera borealis. In*, Würsig, B., Thewissen, J. G. M. and Kovacs, K. M. (eds.) Encyclopedia of Marine Mammals. Academic Press, London, p. 845-847.

Jefferson, T. A., Webber, M. A. and Pitman, R. L. (2015): Marine Mammals of the World. Second Edition. Academic Press, London, 608 pp.

Kato, H. and Perrin W. F. (2018): Bryde's whale, *Balaenoptera edeni. In*, Würsig, B., Thewissen, J. G. M. and Kovacs, K. M. (eds.) Encyclopedia of Marine Mammals. Academic Press, London, p. 143-145.

Kato, H. (1988): Ossification pattern of the vertebral epiphyses in the southern minke whale. *The Scientific Reports of the Whales Research Institute*, (39):11-19.

Kawamura, A. (1980): A review of food of balaenopterid whales. *The Scientific Reports of the Whales Research Institute*, (32):155-197.

Kimura, M. (1989): Measurements of Little piked whale. Nature and Science, (100/101):37-48. [in Japanese]

Kimura, T. and Hasegawa, Y. (2008): Swimming style of the engulfment feeding whales. *Abstracts of the Fifth Conference on Secondary Adaptation of Tetrapods to Life in Water*, 33-34.

Lambert, O. and Muizon, C. de (2013): A new long-snouted species of the Miocene pontoporiid dolphin *Brachydelphis* and a review of the Mio-Pliocene marine mammal levels in the Sacaco Basin, Peru. *Journal of Vertebrate Paleontology*, 33:709-721.

Leslie, M. S., Peredo, C. M. and Pyenson, N. D. (2019): *Norrisanima miocaena*, a new generic name and redescription of a stem balaenopteroid mysticete (Mammalia, Cetacea) from the Miocene of California. *PeerJ*, 7:e7629.

Marx, F. G. and Kohno, N. (2016): A new Miocene baleen whale from the Peruvian desert. *Royal Society Open Science*, 3:160542.

Marx, F. G., Lambert, O. and Muizon, C. de (2017): A new Miocene baleen whale from Peru deciphers the dawn of cetotheriids. *Royal Society Open Science*, 4:170560.

Marx, F. G., Bosselaers, M. E., and Louwye, S. (2016): A new species of *Metopocetus* (Cetacea, Mysticeti, Cetotheriidae) from the Late Miocene of the Netherlands. *PeerJ*, 4:e1572.

Moran, M., Bajpai, S., George, J. C., Suydam, R., Usip, S. and Thewissen, J. G. M. (2015): Intervertebral and epiphyseal fusion in the postnatal ontogeny of cetaceans and terrestrial mammals. *Journal of Mammalian Evolution*, 22:93-109.

Muizon, C. de (1984): Les vertébrés fossiles de la Formation Pisco (Pérou). II: Les Odontocètes (Cetacea, Mammalia) du Pliocène inférieur de Sud-Sacaco. *Institut Français d'Études Andines,Mémoire*, (50):1-188.

Muizon, C. de (1988): Les vertébrés fossiles de la formation Pisco (Pérou) III: Les Odontocètes (Cetacea, Mammalia) du Miocène. *Institut Français d'Études Andines,Mémoire*, (78):1-244.

Muizon, C. de (1993): *Odobenocetops fordycei*: una remarcable convergencia de adaptación alimentaria entre morsa y delfín. *Bulletin de l'Institut Français d'Études Andines*, 22:671-683.

Muizon, C. d. and Bellon, H. (1986): Nouvelles données sur l'âge de la Formation Pisco (Pérou). Comptes Rendus de l'Académie des Sciences. de Paris, 303:1401-1404.

Muizon, C. de. and DeVries, T. J. (1985): Geology and paleontology of late Cenozoic marine deposits in the Sacaco area (Peru). *Geologische Rundschau*, 74:547-563.

Muizon, C. de, Domning, D. P. and Parrish, M. (1999): Dimorphic tusks and adaptive strategies in a new species of walrus-like dolphin (Odobenocetopsidae) from the Pliocene of Peru. *Comptes Rendus de l'Académie des Sciences, series 2* (*Science de la Terre et des Planètes*), 329:449-455.

Nishiwaki, M. and Kasuya, T., 1971: Osteological note of an Antarctic sei whale. *The Scientific Reports of the Whales Research Institute*, (23):83-89.

Ochoa, D., Salas-Gismondi, R., DeVries, T. J., Baby, P., Muizon, C. de, Altamirano, A., Barbosa-Espitia, A., Foster, D. A., Quispe, K., Cardich, J., Gutiérrez, D., Perez, A., Valqui, J., Urbina, M. and Carré, M., 2021: Late Neogene evolution of the Peruvian margin and its ecosystems: a synthesis from the Sacaco record. *International Journal of Earth Sciences*, 110:995-1025.

Ochoa, D., DeVries, T. J., Quispe, K., Barbosa-Espitia, A., Salas-Gismondi, R., Foster, D. A., Gonzales, R., Revillon, S., Berrospi, R., Pairazamán, L., Cardich, J., Perez, A., Romero, P., Urbina, M. and Carré, M. (2022): Age and provenance of the Mio-Pleistocene sediments from the Sacaco area, Peruvian continental margin. Journal of South American Earth Sciences, 116:103799.

Omura, H. (1957): Osteological study of the little piked whale from the coast of Japan. *The Scientific Reports of the Whales Research Institute*, (12):1-21.

Omura, H. (1975): Osteological study of the minke whale from the Antarctic. *The Scientific Reports of the Whales Research Institute*, (27):1-36.

Omura, H., Ichihara, T. and Kasuya, T. (1970): Osteology of pygmy blue whale with additional information on external and the characteristics. *The Scientific Reports of the Whales Research Institute*, (22):1-27.

Omura, H. and Kasuya, T. (1976): Additional information on skeleton of the minke whale from the Antarctic. *The Scientific Reports of the Whales Research Institute*, (28):57-68.

Omura, H., Kasuya, T., Kato, H. and Wada, S. (1981): Osteological study of the Bryde's whale from the central South Pacific and eastern Indian Ocean. *The Scientific Reports of the Whales Research Institute*, (33):1-26.

Omura, H., Ohsumi, S., Nemoto, T., Nasu, K. and Kasuya, T. (1969): Black right whales in the North Pacific. *The Scientific Reports of the Whales Research Institute*, (21):1-78.

Perrin, W. F., Mallette, S. D. and Brownell, R. L. Jr. (2018): Minke whale, *Balaenoptera acutorostrata and B. bonaerensis*. *In*, Würsig, B., Thewissen, J. G. M. and Kovacs, K. M. (eds.) Encyclopedia of Marine Mammals, Academic Press. London, p. 608-613.

Pilleri, G. ed. (1989): Beiträge zur Paläontologie der Cetaceen Perus. Hirnanatomisches Institut, Ostermundigen, Bern, 233 pp.

Pilleri, G. (1990): Beiträge zur Paläontologie der Cetaceen und Pinnipedier der Pisco Formation Perus II. Hirnanatomisches Institut, Ostermundigen, Bern, 240 pp.

Pivorunas, A. (1976): A mathematical consideration on the function of baleen plates and their fringes. *The Scientific Reports of the Whale Research Institute*, (28):37-55.

Pyenson, N. D. and Sponberg, S. N. (2011): Reconstructing body size in

extinct crown Cetacea (Neoceti) using allometry, phylogenetic methods and tests from the fossil record. *Journal of Mammalian Evolution*, 18:269-288.
Sears, R. and Perrin, W. F. (2018): Blue whale, *Balaenoptera musculus. In*, Würsig, B., Thewissen, J. G. M. and Kovacs, K. M. (eds.) Encyclopedia of Marine Mammals. Academic Press, London, p. 110-114.
Segre, P. S., Gough, W. T., Roualdes, E. A., Cade, D. E., Czapanskiy, M. F., Fahlbusch, J. et al. (2022): Scaling of maneuvering performance in baleen whales: larger whales outperform expectations. *Journal of Experimental Biology*, 225:jeb243224.
Struthers, J. (1888): Some points in the anatomy of a *Megaptera longimana* part III. *Journal of Anatomy and Physiology*, 22:629-654.
Takakuwa, Y. (2014): A dense occurrence of teeth of fossil "mako" shark "*Isurus*" *hastalis*: Chondrichthyes, Lamniformes), associated with a balaenopterid-whale skeleton of the Late Miocene Pisco Formation, Peru, South America. *Bulletin of the Gunma Museum of Natural History*, (18):77-86. [in Japanese with English abstract]
Tanaka, Y. and Watanabe, M. (2019): An early and new member of Balaenopteridae from the upper Miocene of Hokkaido, Japan. *Journal of Systematic Palaeontology*, 17:1417-1413.
Tanaka, Y., Nagasawa, K. and Taketani, Y. (2020): A new skull of an early diverging rorqual (Balaenopteridae, Mysticeti, Cetacea) from the late Miocene to early Pliocene of Yamagata, northeastern Japan. *Palaeontologia Electronica*, 23:a12. https://doi.org/10.26879/1002
Tanaka, Y., Ohara, M. and Kimura, T. (2019): A large fossil baleen whale from the Shikiya Formation (early middle Miocene) of Wakayama, Japan. *Paleontological Research*, 23:199-207.
True, F. W. (1904): The whalebone whales of the western north Atlantic compared with those occurring in European waters. *Smithsonian Contributions to Knowledge*, (33):1-332.
Walsh, B. M. and Berta, A. (2011): Occipital ossification of balaenopteroid mysticetes. *The Anatomical Record*, 294:391-398.
Young, S. A. (2012): The comparative anatomy of baleen: evolutionary and ecological implications. San Diego State University, San Diego, 111 pp.

ペルーの上部中新統より産出した新種のナガスクジラ類*Incakujira fordycei*

木村敏之[1]・長谷川善和[1, 2]

[1]群馬県立自然史博物館：〒370-2345 群馬県富岡市上黒岩1674-1

（kimura@gmnh.pref.gunma.jp, hasegawa@gmnh.pref.gunma.jp）

[2]飯田市美術博物館：〒395-0034 長野県飯田市追手町2-655-7

要旨：本論文ではペルー共和国の上部中新統ピスコ層より産出したナガスクジラ類化石を報告する．本標本はほぼ全身の骨格が生体時の関節状態を保って保存され，かなり広い部分に軟質部の痕跡が，さらに頭蓋には多数の連続したクジラヒゲの痕跡が確認できるなど，非常に保存状態の良い化石標本である．本論文ではこの標本を*Incakujira*属の新種*I. fordycei*として報告する．この標本によってナガスクジラ類の形態的多様性や古生物地理的な情報が新たに明らかとなるとともに，本標本の椎骨やクジラヒゲの形態の検討から，*I. fordycei*は機敏な遊泳能力を持ち，多様な餌生物を捕食していたことが示唆される．

キーワード：クジラ類，ヒゲクジラ類，ナガスクジラ科，*Incakujira fordycei*, 中新世，ペルー，ピスコ層